Bulletin of the JSME Vol.12, No.5, 2025
Mechanical Engineering Journal

Examining OpenFOAM-based LES analysis in terms of inviscid energy conservation and viscous turbulence decay

Hiroki SUZUKI*, Kento TANAKA* and Toshinori KOUCHI*
*Graduate School of Environmental, Life, Natural Science and Technology, Okayama University
3-1-1 Tsushima-naka, Kita-ku, Okayama-shi, Okayama 700-8530, Japan
E-mail: h.suzuki@okayama-u.ac.jp

Received: 27 March 2025; Revised: 15 June 2025; Accepted: 10 September 2025

Abstract
The present study examines an OpenFOAM-based LES analysis from the viewpoints of inviscid energy conservation and viscous turbulence decay. The Smagorinsky model is employed as the sub-grid scale (SGS) model, and a two-dimensional periodic analytical solution and a three-dimensional periodic Taylor-Green vortex (TGV) are employed to represent inviscid flows. The analytical relationship for the kinetic energy K, $dK/dt = 0$, with t as the dimensionless time, is utilized to validate the OpenFOAM results. For the viscous flow case, the TGV flow in a three-dimensional periodic cubic domain is adopted, and its turbulence kinetic energy distribution is compared with that obtained by a spectral method to examine the analysis. The OpenFOAM-based analysis exhibits energy conservation error in flows that should ideally conserve energy. For the two-dimensional flow, this error decreases with increasing grid resolution N. However, in the three-dimensional flow, the error does not improve even with higher N. In the three-dimensional TGV flow, the turbulence kinetic energy predicted by OpenFOAM exhibits a strong agreement with that from the spectral method when a standard constant value of the Smagorinsky model is employed and the mesh is sufficiently refined. Conversely, for a condition of relatively coarse mesh, the decay characteristics of turbulent kinetic energy deviate from those of the spectral method, and a higher constant value of the Smagorinsky model than the default value becomes necessary to reproduce comparable results. These results suggests that even in LES simulations where highly accurate conservation laws are not satisfied, adjusting the model constants so that the predicted values match experimental or numerical reference data can improve the apparent reliability of the turbulent kinetic energy in the decaying turbulence.

Keywords : Turbulent flows, Numerical simulation, Large-eddy simulation, Energy conservation, Decaying turbulence

1. Introduction

Incompressible turbulent phenomena are frequently observed in flows around transportation vehicles and in atmospheric environments, requiring highly accurate numerical analysis (Pope, 2000). Compared to Reynolds-averaged Navier-Stokes (RANS) models (Spalart, 2000; Menter, 2009; Xiao and Cinnella, 2019), large-eddy simulation (LES) has the advantage of directly resolving large-scale turbulent eddies, allowing for a more refined capture of unsteady flow phenomena (Meneveau and Katz, 2000). However, uncertainties due to model parameters and mesh resolution are unavoidable in LES (Canuto and Cheng, 1997; Park et al., 2006), and high accuracy is not always guaranteed. Therefore, it is essential to validate LES predictions by comparing them with experimental data and direct numerical simulations (DNS) to clarify the applicability and limitations of the method. In particular, while RANS often struggles to adequately represent complex turbulent structures and vortex generation (Shirzadi et al., 2020; Brener et al., 2021; Song et al., 2022), LES is considered highly effective for such flow regimes. Nevertheless, continuous evaluation is crucial to ensure the accuracy of LES, and it is imperative to accumulate further verification evidence to increase its reliability.

Paper No.25-00095
J-STAGE Advance Publication date : 20 September, 2025
[DOI: 10.1299/mej.25-00095]

A key factor that significantly influences the high fidelity of incompressible LES analyses is the energy conservation property (Harlow and Welch, 1965; Morinishi et al., 1998). This property concerns the conservation properties of the transport equations for turbulent kinetic energy and velocity fluctuation intensities derived from the discretized governing equations. Ideally, these properties should be preserved in the same way as in the original continuous equations. Attention has long been paid to this perspective, and second-order accurate discretization for the convective terms have been employed (Harlow and Welch, 1965). Subsequently, generalized higher-order discretization schemes have been developed, often based on fractional-step methods, and their energy conservation properties are often verified in inviscid periodic flow problems (Morinishi et al., 1998). As conservation errors occur, it has been found that inaccuracies in static pressure fluctuations can exceed those in turbulent kinetic energy (Honda et al., 2021). Unlike the reduction in spatial resolution typically caused by discretization errors (Morinishi and Vasilyev, 2002; Suzuki and Hasegawa, 2024), these conservation errors can be difficult to compensate for using subgrid-scale (SGS) models (Chitose et al., 2024). Although any discretization approach inevitably introduces some numerical error, increasing the order of accuracy is expected to yield results that asymptotically approach those of spectral methods. In this context, compact difference schemes, widely used in compressible flow analysis, have also been subjected to similar examination (Morinishi et al., 2011).

In recent years, general purpose solvers have been widely used for LES, among which OpenFOAM is a notable example (Jasak, 2009). Numerous studies have reported scientific results obtained through OpenFOAM-based LES analyses (Constant et al., 2017; Xia et al., 2020). For example, incompressible flows around bluff bodies have been simulated with OpenFOAM and compared with FLUENT software (Robertson et al., 2015). Furthermore, the accuracy and validity of OpenFOAM-based LES was confirmed in the wake of a circular cylinder (Cao and Tamura, 2016; Jiang and Cheng, 2021; Muhammad et al., 2022). In the same flow configuration, the influence of different subgrid-scale (SGS) models on the OpenFOAM LES results was investigated, as well as the influence of mesh element shapes on the circular cylinder wake simulation. OpenFOAM-based turbulence analyses were also validated on channel and pipe flows (Komen et al., 2014), which served as benchmark cases for high-fidelity simulations. In these validations, quasi-direct numerical simulations with OpenFOAM accurately reproduced the fundamental statistical properties of wall-bounded turbulent flows. Other studies have also reported that OpenFOAM-based LES is capable of capturing the low-order statistical quantities in channel flows with satisfactory accuracy (LarKermani et al., 2018).

As highlighted in the previous studies show above, the fact that the energy conservation property under inviscid conditions can significantly influence LES fidelity (e.g., Morinishi et al., 1998) is presumably also true for OpenFOAM-based LES. However, to the extent of the current knowledge, the energy conservation properties of OpenFOAM-based LES have not been explicitly investigated in existing research. As a result, the energy conservation perspective has been missing when investigating the accuracy of OpenFOAM-based LES, and it remains uncertain whether OpenFOAM can reliably handle inviscid flow conditions. The previous validation efforts for OpenFOAM simulations have mainly focused on wall-bounded flows and flows around bluff bodies. Meanwhile, high-fidelity analyses have used not only wall-bounded flows but also free-stream turbulence to validate simulation accuracy. The present study argues that OpenFOAM-based LES should also be tested using such the decaying turbulence. In particular, wind tunnel experiments have investigated one of the most fundamental properties of turbulence, the decay characteristics, and quantified it by a decay exponent (Pope, 2000; Mohamed and LaRue, 1990; Krogstad and Davidson, 2010; Kurian and Fransson, 2009; Suzuki et al., 2016). Since this exponent is one of the parameters in RANS models (Pope, 2000), testing OpenFOAM on this property has practical engineering relevance. When evaluating turbulence decay characteristics, it is noteworthy that the Taylor-Green Vortex (TGV) flow (Brachet et al., 1983; Drikakis et al., 2007) has often been used in previous studies (Shu et al., 2005; Lehmkuhl et al., 2019; Asada et al., 2024). However, examples of OpenFOAM-based LES applied to TGV flows appear to be rather limited (Kajzer et al., 2014).

The objective of this study is to examine OpenFOAM-based LES analyses in terms of inviscid energy conservation and turbulent viscous decay. As inviscid flow fields, a two-dimensional periodic flow field described by Taylor's analytical solution (Kim and Moin, 1985; Suzuki et al., 2017) and a three-dimensional periodic flow field given by the Taylor-Green vortex (TGV) (Brachet et al., 1983; Drikakis et al., 2007) are used. In these flow fields, the kinetic energy is theoretically conserved at a constant level, and thus they are often used in previous studies to investigate energy conservation properties. As shown in this work, OpenFOAM exhibits a non-negligible conservation error in three-dimensional inviscid flow. With respect to turbulent viscous decay, the focus is on the decay law of turbulent kinetic energy in a fully developed three-dimensional TGV flow, with particular emphasis on the decay exponent. The results of the present OpenFOAM-based LES analyses for the three-dimensional TGV flow are compared with those obtained from

[DOI: 10.1299/mej.25-00095]

DNS using a Fourier spectral method (Canuto et al., 1988; Suzuki and Kouchi, 2022) and from the finite difference method conserving energy under inviscid conditions. As shown here, the turbulent kinetic energy distributions of the OpenFOAM-based LES do not agree with those of the reference analyses when the default Smagorinsky model constant is used. However, this discrepancy can be mitigated by assigning a model constant value larger than the default setting. The present work addresses OpenFOAM-based large-eddy simulation (LES) from an engineering perspective rather than fundamental turbulence research, and therefore does not consider direct numerical simulation (DNS). LES lowers computational cost in unsteady-flow calculations by modelling motions whose spatial scales fall below the grid spacing, allowing a coarser mesh. Because engineering analyses commonly require such cost reductions, LES is often practicable, whereas DNS is typically prohibitive. When DNS is warranted, one can invoke solvers that incur no kinetic-energy conservation error—such as the Fourier spectral method employed here—without relying on OpenFOAM, whose discretisation may introduce non-negligible conservation errors. Consequently, while rigorous verification of OpenFOAM-based LES is essential for engineering use, validating OpenFOAM as a DNS platform is of markedly lower priority. For these reasons, the present study confines its scope to the verification of OpenFOAM-based LES.

2. Examination in terms of inviscid energy conservation

2.1 Methods

In this section, the inviscid flows are considered within two-dimensional and three-dimensional periodic domains. In an inviscid, incompressible flow, the kinetic energy of the system is conserved provided that no boundaries or external forces are present. Upholding this energy-conservation law in LES is pivotal, because it ensures that the discrete governing equations honour the fundamental physics of the continuous system. When a discretisation scheme lacks strict energy conservation, the theoretically guaranteed energy cascade can be distorted, impairing the correct transfer of kinetic energy from large to small eddies. By preventing spurious numerical dissipation or production, an energy-preserving scheme allows the cascade process to proceed in accordance with physical principles. If the numerical method conserves energy, the decay of turbulent kinetic energy is driven solely by molecular viscosity and SGS model; consequently, the computed energy spectrum and turbulence intensity remain realistic. The improved prediction of statistics at energy-containing scales enhances the physical fidelity and internal consistency of LES results. Maintaining a proper energy budget at each scale therefore permits reliable turbulence analyses. Moreover, spatial discretisations endowed with energy-preserving properties suppress non-physical energy growth, leading to enhanced numerical stability. This feature is especially valuable in applications—such as atmospheric turbulence or wind-farm flows—in which molecular viscosity is often neglected and the governing equations reduce to inviscid form. Balancing energy conservation with stability enables robust long-time integrations without resorting to excessive numerical viscosity. For these reasons, energy conservation in LES has been a topic of active research for more than sixty years and remains a pressing issue today. Ongoing developments that reconcile conservation accuracy with computational efficiency will be indispensable for future high-fidelity simulations

The computational domains for the two- and three-dimensional flows are a square and a cube, respectively, each with a side length of 2π (Ono et al., 2025). The origin of the coordinate system is placed in the center of these domains, and for x, y and z directions are defined accordingly. The OpenFOAM simulations conducted in this study employ a structured mesh with periodic boundary conditions applied in all directions. The solver is implemented using OpenFOAM's native finite-volume formulation. In the present study, all simulations of the OpenFOAM were carried out with OpenFOAM v2106. The governing equations are the continuity equation for incompressible flow and the inviscid Navier-Stokes equations for the velocity components, u, v and w for x, y and z directions. As described later, these equations incorporate the subgrid scale (SGS) shear stresses associated with an LES approach, and by allowing the SGS stresses to asymptotically approach zero, this setup allows us to investigate whether inviscid flow can be reproduced. Consequently, the governing equations are considered to have been subjected to a filtering operation. The primary motivation for focusing on inviscid flows is to exploit the analytically known conservation of kinetic energy under inviscid conditions, following a similar rationale in previous studies (Morinishi et al., 1998; Honda et al., 2021; Chitose et al., 2024). For the two-dimensional inviscid flow, the Taylor analytic solution given below is used as the initial condition (Suzuki et al., 2017):

$$u(x,y) = 2\cos(x)\sin(y) \text{ and } v(x,y) = -2\sin(x)\cos(y). \quad (1)$$

[DOI: 10.1299/mej.25-00095]

Under inviscid conditions, the above flow field remains constant in time. This solution can be derived by imposing inviscid constraints on the original Taylor solution for viscous flows. For the three-dimensional inviscid flow, we use the Taylor-Green vortex (TGV) field, which is commonly used to validate numerical schemes. The initial velocity field of the TGV flow is given as follows (Brachet et al., 1983):

$$u(x,y,z) = 2\sqrt{2}\cos(x)\sin(y)\cos(z),\ v(x,y,z) = -2\sqrt{2}\sin(x)\cos(y)\cos(z),\ \text{and}\ w(x,y,z) = 0. \quad (2)$$

Here, $(u,v,w) = (u_1,u_2,u_3)$ for x_i directions with $i = 1, 2, 3$, where $(x,y,z) = (x_1,x_2,x_3)$. As can be seen from the above expressions, the constant in the initial velocity field is chosen such that the spatially averaged kinetic energy, denoted by K, is $K = 1$. This flow field is used to validate the present OpenFOAM-based analysis. The PISO algorithm is used to solve the system of governing equations (Komen et al., 2014), consistent with a previous study that validated an OpenFOAM simulation for turbulent channel flow. The BiCGStab method is used for the convergence. In the present analysis, subgrid scale (SGS) stresses are retained in the governing equations, and by gradually reducing the Smagorinsky model constant toward zero, we aim to replicate an inviscid flow. Specifically, we use the Smagorinsky model whose constant is denoted by C_s. Here, SGS eddy viscosity of the Smagorinsky model ν_{SGS} is obtained as $\nu_{SGS} = (C_s\Delta)^2\,\bar{S}$, where $\bar{S}$ is the characteristic filtered rate of strain, obtained as $\bar{S} = (2\,S_{ij}\,S_{ij})^{1/2}$ with $S_{ij} = (1/2)\,(\partial u_i/\partial x_j + \partial u_j/\partial x_i)$ (Pope, 2000) , where S_{ij} and u_i are provided as the filtered quantities, and Δ is the filter length scale, set to be equal to the grid width. Four values of C_s are considered in this study: 0.01, 0.001, 0.0001, and 0. Because advance certainty could not be obtained that stable computations would be possible at $C_s = 0$, simulations were carried out not only for $C_s = 0$ but also for cases in which C_s was asymptotically reduced toward zero. A second order Crank-Nicolson scheme (Choi and Moin, 1994) is used for time integration. In the present work, the nonlinear terms in the coupled governing equations are advanced in time with a Crank–Nicolson scheme embedded within a PISO algorithm. Here, in OpenFOAM's PISO algorithm, the eddy-viscosity coefficient is computed once per time step and treated as a fixed value during the velocity–pressure iterations of the PISO loop; this is the standard procedure. The use of PISO follows the approach of Komen et al. (2014); however, those authors did not employ Crank–Nicolson for temporal discretization. Guided by earlier studies that advocate Crank–Nicolson for both viscous and nonlinear terms (e.g., Choi and Moin, 1994), we adopt the same second-order scheme here. Also, spatial derivatives are approximated by a second order central difference method. Both schemes are the same as those used in the previous study. For both two- and three-dimensional cases, the number of grid points per side N is varied among 10, 32, and 100. The time step Δt is set to 0.005 and the simulation is run until $t = 20$. Additionally, we assessed time-step sensitivity in the three-dimensional inviscid Taylor–Green vortex by successively reducing the step size to $\Delta t = 0.015$, 0.010, and 0.005. The initial kinetic-energy gradient—which reflects the conservation error—decreased monotonically as Δt was refined. The purpose of the inviscid tests was to evaluate the numerical schemes implemented in OpenFOAM, chiefly its spatial and temporal discretisations, rather than to validate the physical turbulence model used in the LES framework. Indeed, only the Smagorinsky SGS model is employed in the present study, so verification of the turbulence-modelling strategy lies outside the current scope. Because OpenFOAM is known to exhibit non-negligible kinetic-energy conservation errors under inviscid conditions, we anticipated that its stability might deteriorate and, in the worst case, the calculation might diverge. To explore this possibility, the governing equations were solved without the viscous term while the Smagorinsky constant C_s was progressively reduced to zero, thereby removing both the molecular viscosity and the SGS eddy viscosity in the asymptotic limit. Kinetic-energy conservation errors can manifest in two distinct ways: (i) a monotonic increase in energy leading to numerical blow-up, or (ii) a gradual loss of energy with time. In our OpenFOAM runs the latter behaviour was observed—the mean kinetic energy decreased steadily, but no divergence occurred, and the solver remained stable throughout the simulation window. Consequently, although OpenFOAM does not preserve kinetic energy exactly, the code proved capable of executing inviscid LES calculations without numerical breakdown even when both molecular and SGS viscosities were completely absent.

2.2 Results and discussion

The present study begins with the results concerning the convergence of the two-dimensional flow to an inviscid state. Figure 1 shows contour plots of the kinetic energy illustrating the dependence on the Smagorinsky model constant C_s. Here the results are shown for $N = 32$. As C_s decreases, the flow field approaches an inviscid regime, and at $C_s = 0$ it

[DOI: 10.1299/mej.25-00095]

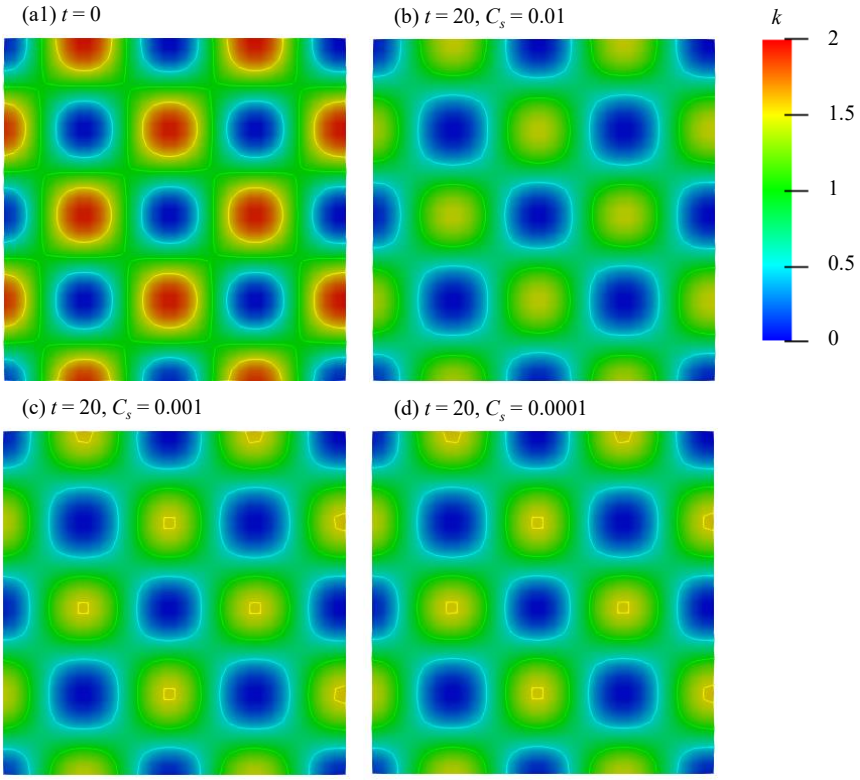

Fig. 1 Dependence of the kinetic energy distribution of the two-dimensional (2D) flow described by Taylor's analytical solution on the model constant C_s. Here $N = 32$. Panel (a1) shows the initial energy field. As the figure shows the distributions obtained with $C_s = 0.001$ and $C_s = 0.0001$ are visually indistinguishable.

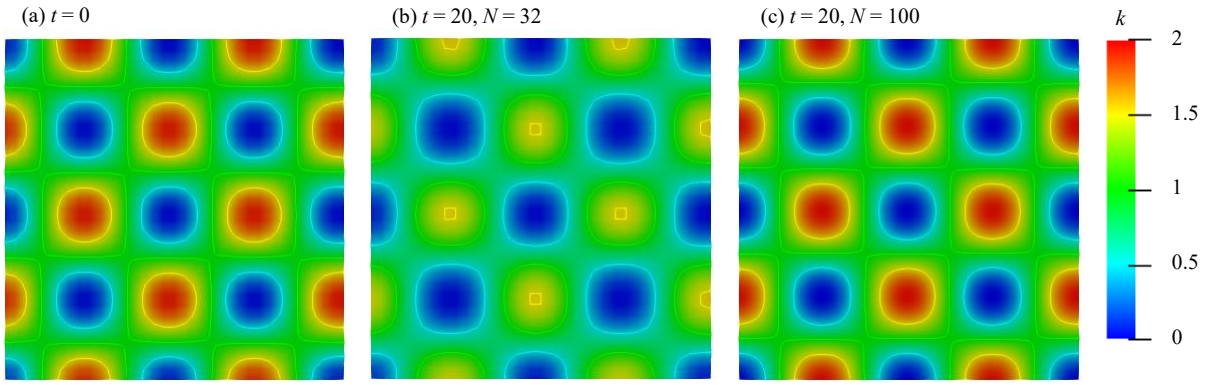

Fig. 2 Grid dependence of the kinetic energy distribution for the inviscid 2D flow described by Taylor's analytical solution. Here, $C_s = 0$ (the inviscid condition), and panel (a) shows the initial energy field. As shown in panels (b) and (c), at $t = 20$ the energy field remains closer to the initial condition for larger N.

reduces to a strictly inviscid flow. As can be seen in Fig. 1(a), the initial flow field is characterized by an alternating spatial pattern of high and low energy regions. The contour plots of the kinetic energy at $t = 20$ are shown in Fig. 1(b)-(d). As can be seen, the alternating pattern of high and low energy regions seen in the initial state is maintained at $t = 20$. The flow field is expected to converge as C_s is reduced. Indeed, the results for $C_s = 0.001$ in Fig. 1(c) are quantitatively similar to those for $C_s = 0.0001$ in Fig. 1(d). On the other hand, Fig. 1(b), where = 0.01, shows a noticeable quantitative discrepancy compared to Fig. 1(d). Figure 2 shows the two-dimensional contour plots of the kinetic energy at $C_s = 0$, corresponding to the inviscid condition, and highlights the dependence on the number of grid points N. Figure 2(a) shows the initial flow field at $t = 0$. As the figure shows, even under the inviscid condition, $C_s = 0$, the kinetic energy contours show a clear dependence on N. In particular, for $N = 100$ at $t = 20$ shown in Fig. 2(c), the contour distribution closely

[DOI: 10.1299/mej.25-00095]

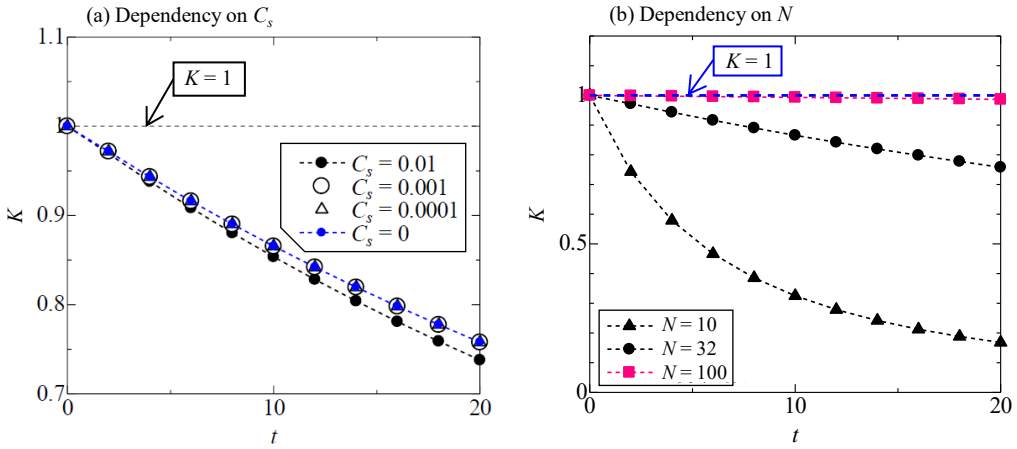

Fig. 3 Dependence of the mean kinetic energy distribution of the 2D flow described by Taylor's solution on C_s and N). (a) Dependence on C_s. Here $N = 32$. As C_s to 0, the energy distribution converges. (b) Dependence on N. As N increases, the distribution approaches that of the analytical solution.

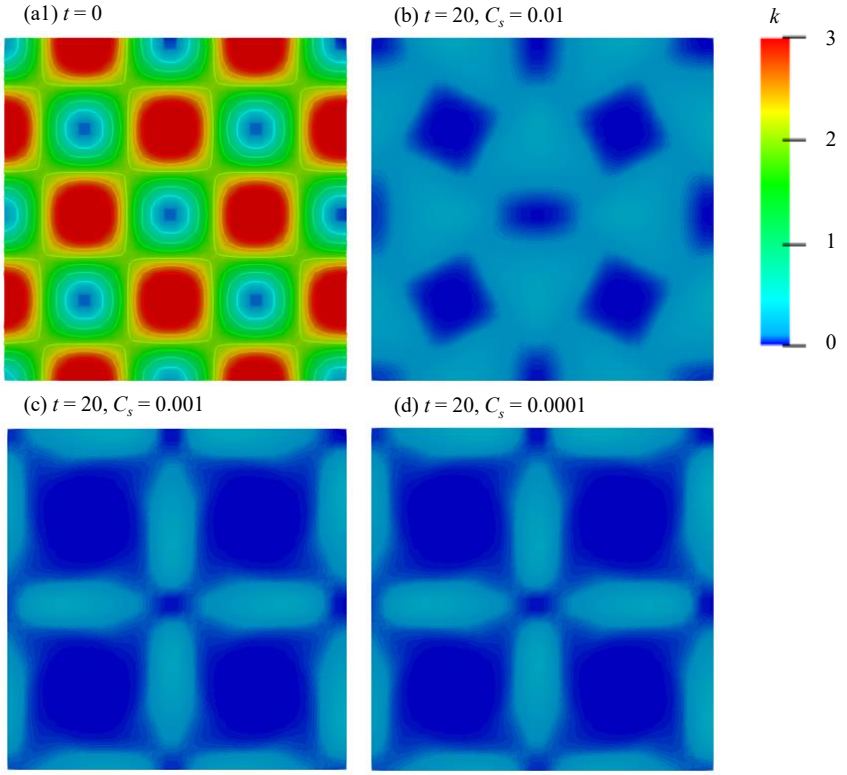

Fig. 4 Contours of the kinetic energy in the three-dimensional (3D) Taylor-Green vortex (TGV) flow, showing the dependence on C_s. These contour plots are taken at $z = \pi$. Panel (a) shows the initial field. As can be seen in panels (b)-(d), the contours converge as C_s to 0.

resembles that of the initial field, suggesting that kinetic energy errors in the two-dimensional flow may be small at this resolution. In contrast, for $N = 32$ in Fig. 2(b), the $t = 20$ contours differ significantly from those of the initial field. This comparison implies that the degree of kinetic energy conservation in the present OpenFOAM analysis is influenced by the grid resolution.

Figure 3 shows the time evolution of the spatially averaged kinetic energy K for different values of C_s and different numbers of grid points N. In the figure, the line $K = 1$ indicates the analytically expected energy conservation under inviscid conditions. As shown in Fig. 3(a) for the case $N = 32$, the energy distribution converges as C_s approaches zero. Notably, OpenFOAM produces valid simulation results for every tested value of C_s that tends to zero, indicating that OpenFOAM is indeed capable of analyzing a two-dimensional periodic inviscid flow. In the present study, which

[DOI: 10.1299/mej.25-00095]

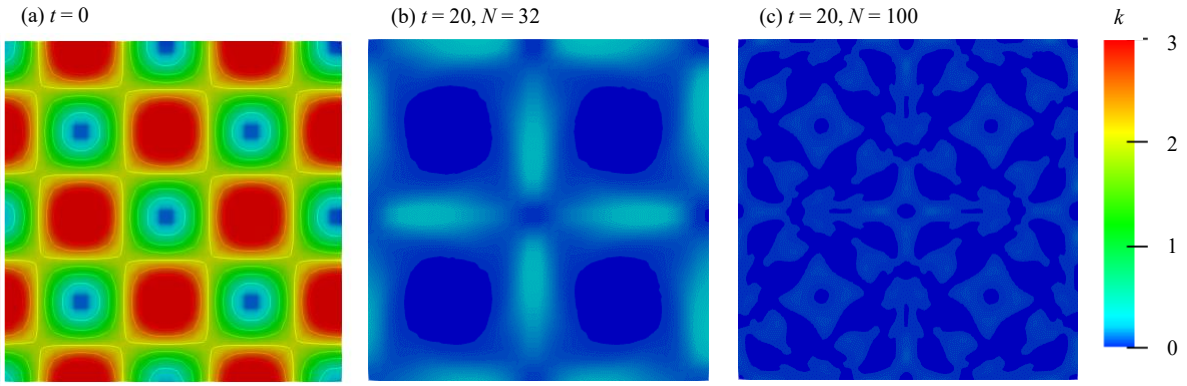

Fig. 5 Contours of kinetic energy in the 3D inviscid TGV flow, showing the dependence on the number of grid points N. Similarly, these contours are plotted at $z = \pi$, and panel (a) shows the initial field. As shown in panels (b) and (c), the contours at $t = 20$ have extensive blue regions corresponding to low wavenumbers that differ from the initial field.

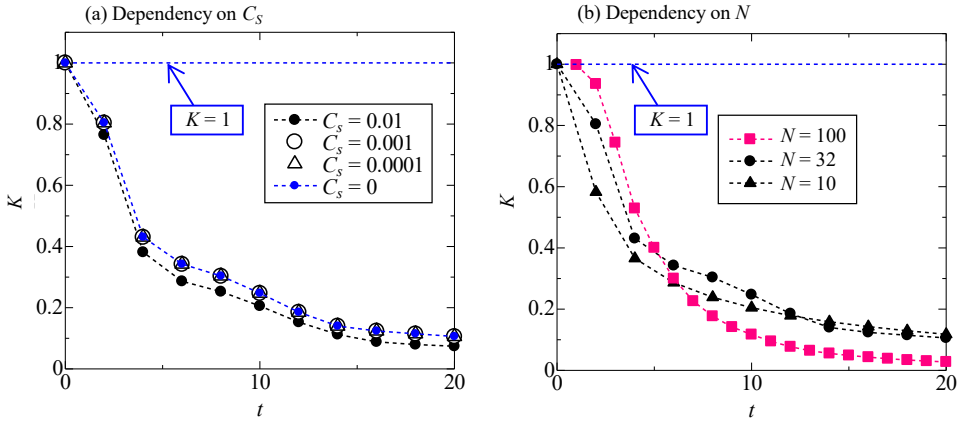

Fig. 6 Dependence of the mean kinetic energy distribution in the 3D TGV flow on C_s and N. (a) C_s dependence. The distribution converges as C_s to 0. Here $N = 32$. (b) N dependence, under the inviscid condition ($C_s = 0$). As shown, even with increasing N, the distribution does not converge to the analytical value $K = 1$.

investigates whether OpenFOAM satisfies the kinetic-energy conservation law, it was not evident beforehand whether a solver that may contain conservation errors could remain stable under genuinely inviscid conditions—namely, with the viscous term suppressed and the Smagorinsky model constant set to zero. Because schemes that strictly conserve kinetic energy in the inviscid limit typically exhibit robust numerical stability, the inviscid tests were designed by gradually reducing the SGS constant toward zero while disabling the viscous term. The calculations reveal that OpenFOAM converges without divergence even when the viscous term is omitted and the SGS constant is set exactly to zero. Figure 3(b) shows the dependence of the time evolution of K on N. As can be seen, for $N = 10$ and $N = 32$ the averaged kinetic energy decreases with time. In contrast, for $N = 100$ the time evolution of K remains close to unity. These results confirm that, for two-dimensional flows, the accuracy of kinetic energy conservation in OpenFOAM improves with increasing number of grid points.

Next, the results for the inviscid three-dimensional TGV flow are shown. Figure 4 shows the contour plots of the kinetic energy at $z = \pi$, illustrating the dependence on the Smagorinsky model constant C_s. The initial flow field at $t = 0$ is shown in Fig. 4(a). As can be seen, the contours at $t = 20$ converge as C_s approaches zero, and the results for $C_s = 0.001$ appear to coincide with those for $C_s = 0.0001$. In contrast, the contours at $t = 20$ for $C_s = 0.01$ deviate visibly from those obtained with the two smaller C_s values. Figure 5 shows the dependence of the kinetic energy distribution on the number of grid points for the inviscid TGV flow obtained by the present OpenFOAM-based analysis. As before, these contour plots are taken at $z = \pi$, and Fig. 5(a) shows the initial flow field. Note that the color scale used in this figure is different from that used in the previous figures. The colour scale in Fig. 4 is linear in the displayed values. Under this palette, however, the spatial distribution of kinetic energy in Fig. 5 (c) is not rendered with sufficient contrast. Because that distribution reflects the time-dependent evolution of the flow structures, clear visualisation is essential. Accordingly, in

[DOI: 10.1299/mej.25-00095]

Fig. 5 (c) we adjusted the colour mapping in the vicinity of zero kinetic energy, allowing the field to be presented as a contour plot that more clearly reveals its spatial variation. As shown in Fig. 5(b) and (c), at $t = 20$, the contour plots for both grid resolutions are predominantly in the blue region. This indicates that throughout the domain, the kinetic energy at $t = 20$ has decreased by a non-negligible amount from its initial distribution, and that this decay appears to be relatively insensitive to changes in the number of grid points N.

Figure 6 shows the temporal evolution of the spatially averaged kinetic energy K for the inviscid three-dimensional TGV flow, illustrating its dependence on both the Smagorinsky model constant C_s and the number of grid points N. In each panel, the line $K = 1$ denotes the analytically expected value under truly inviscid conditions. As can be seen in Fig. 6(a) for $N = 32$, the energy distribution converges to the $C_s = 0$ result as C_s decreases. This finding suggests that OpenFOAM can indeed perform simulations under inviscid conditions for the three-dimensional TGV flow in a manner consistent with the two-dimensional inviscid flow results. This remark explains that, for the three-dimensional inviscid flow—just as for the two-dimensional case—the computation could still be performed with $N = 32$ even after the SGS coefficient was progressively reduced to $C_s = 0$; however, kinetic energy was not conserved under those conditions. Figure 6(b) shows the dependence of the kinetic energy distribution on the number of grid points. Even with increasing N, thus decreasing the grid size, the averaged kinetic energy does not approach the analytically expected $K = 1$, but rather shows a non-negligible deviation. This behavior is in contrast to the two-dimensional case, where the conservation error decreases with increasing mesh resolution.

In the two-dimensional flow, the inviscid Taylor analytical solution was employed; for the viscous Taylor solution, the viscous term balances the unsteady term, and the convective term balances the pressure term (e.g., Suzuki et al., 2017). When the viscous term is absent, the unsteady term becomes zero, whereas the balance between the convective and pressure terms still holds. The same balance between the convective and pressure terms is presumed to persist even in the presence of conservation errors. This can be confirmed from the close similarity between Fig. 2(c), which includes conservation error, and Fig. 2(a). Because the PISO algorithm in OpenFOAM introduces a small error into the continuity equation, these two equilibrium relations are not exact but approximate, as pointed out in previous studies. The non-zero unsteady term is considered to originate from an error term whose magnitude decreases with increasing grid resolution. When such an equilibrium exists among the terms other than the error term and the error term merely appears as an additional unsteady term, the solver is expected to produce valid results; such situations are frequently observed in laminar flows. By contrast, in a three-dimensional inviscid field, the balance between the convective and pressure terms is not expected to hold at every location. In this case, the error term influences the flow field through its effect on the convective term, and consequently the kinetic energy is affected. Here, in this study, the Δt-dependence of the kinetic-energy conservation error in 3D cases does not coincide with the second-order accuracy of the Crank–Nicolson method; instead, the observed exponent is smaller than two. Although the time-step dependence of this error is of interest, the procedure for quantifying its Δt-dependence requires further investigation. Therefore, these results are not included in the present work.

3. Examination in terms of viscous turbulence decay

3.1 Methods

The turbulent flow under consideration is reproduced in a three-dimensional periodic cubic domain of side length 2π. The governing equations are the continuity equation for incompressible flow and the Navier-Stokes equation, both nondimensionalized using a Reynolds number of Re = 1600 (Suzuki and Kouchi, 2022). These filtered equations contain subgrid-scale (SGS) shear stresses that need to be modeled. In this study, as in the analysis of three-dimensional inviscid flow presented in the previous chapter, we adopt the widely used Smagorinsky model in OpenFOAM-based LES to model the SGS shear stresses. The initial velocity field is given by the Taylor-Green vortex (TGV) formulation, identical to Eq. (2) introduced earlier. Furthermore, the algorithm, time integration scheme, and spatial discretization used here to analyze the viscous turbulent flow in OpenFOAM are the same as those discussed previously. The number of grid points per dimension, N, is set to $N = 32$, which is commonly chosen resolutions in previous LES studies (Kobayashi, 2005), or $N = 128$. In the present OpenFOAM-based analysis, the Smagorinsky model constant C_s takes the values $C_s = 0$, 0.1, 0.2, 0.3, 0.4, 0.5, and 0.6 for $N = 32$, while for $N = 128$, $C_s = 0$, 0.1, 0.2, and 0.3, based on previous studies (Pope, 2000; Canuto and Cheng, 1997; Park et al., 2006).

The results of the present OpenFOAM-based analysis are compared with those of a spectral method and an LES analysis based on a fractional-step method instead of OpenFOAM. The spectral method follows a standard formulation

[DOI: 10.1299/mej.25-00095]

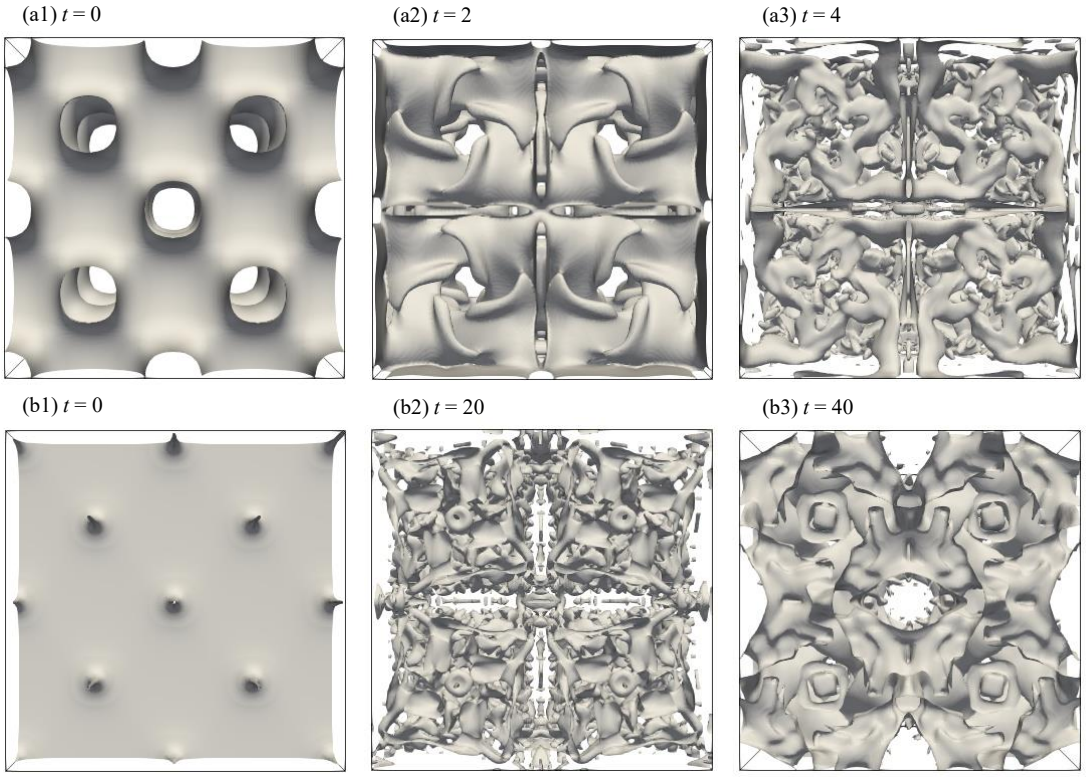

Fig. 7 Time evolution of isosurfaces of turbulent kinetic energy k for the 3D viscous TGV flow obtained by the present OpenFOAM analysis. The depth (into the sheet) is the z direction, while the horizontal and vertical directions are x and y, respectively. Panels (a1)-(a3) show the isosurface of $K = 1$ at $t = 0$, 2, 4. Panels (b1)-(b3) show the isosurface of $k = 0.005$ at $t = 0$, 20, 40. Although the present OpenFOAM solver exhibits certain conservation errors under the inviscid condition, the evolving instantaneous flow fields maintain symmetry.

(Canuto et al., 1988) verified in the previous study (Suzuki and Kouchi, 2022). Specifically, the pressure is eliminated using the projection tensor with an integrating factor approach for the viscous term and a five-step fourth-order Runge-Kutta scheme for the inertial term. The 2/3 rule is used to mitigate aliasing. The spatial grid size for the spectral method is $N = 256$. The governing equations in the fractional-step LES analysis are the same as in the OpenFOAM-based approach; however, instead of the PISO algorithm, a fractional-step method is used to solve the system of equations (Suzuki et al., 2013a, 2013b). In this framework, the Poisson equation is solved at each fractional step using a direct method based on fast Fourier transform (Suzuki and Hasegawa, 2024). A fourth-order conservative central-difference scheme (Morinishi et al., 1998) is used on a staggered grid with $N = 32$ grid points per dimension. For time integration, a five-step fourth-order Runge-Kutta method (RK4) (Suzuki et al., 2020), a second-order Adams-Bashforth method (AB2), or a second-order Crank-Nicolson method (CN2) is used. Notably, the second-order Crank-Nicolson scheme, unlike the two explicit time integration schemes, does not preserve energy under inviscid conditions. In the fractional-step LES analysis, the Smagorinsky model constant C_s takes the values 0.1, 0.12, 0.4, and 0.5. Because Morinishi's energy-conserving formulation is explicit in time, a truncation error in the kinetic-energy budget is unavoidable. Extensive work by the first author has demonstrated that this error is negligibly small. For instance, with a staggered grid and a fourth-order Runge–Kutta integrator, the deviation from exact conservation converges to machine precision (Suzuki et al., 2020a). The same verified configuration is employed in the latter part of the present manuscript for the Taylor–Green vortex and serves as the reference solution. On a collocated grid, the conservation error can be improved to second-order accuracy in time (Suzuki et al., 2020b).

3.2 Results and discussion

Figure 7 shows a visualization of the TGV flow field obtained from the current OpenFOAM-based LES analysis using isosurfaces of kinetic energy $u_i u_i/2$. The results correspond to the case $N = 128$. In the figure, the depth (into the sheet) direction is z, while the horizontal and vertical axes are x and y, respectively. Figure 7(a1)-(a3) shows the time

[DOI: 10.1299/mej.25-00095]

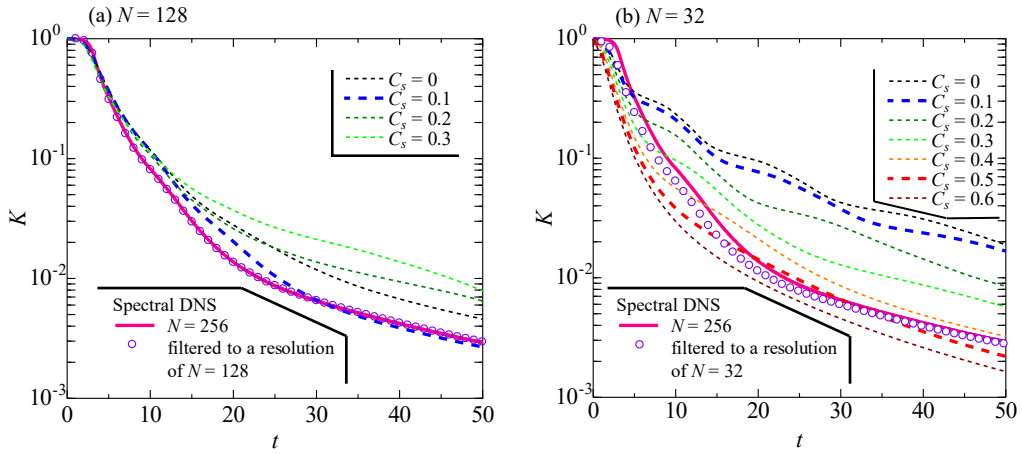

Fig. 8 Time evolution of turbulent kinetic energy for the 3D viscous TGV flow obtained by the present OpenFOAM analysis. Here K is the spatially averaged value at each time. The OpenFOAM results are plotted as a function of C_s and compared with those from a spectral method. (a) Case $N = 128$. The distribution of K from the OpenFOAM analysis with the default C_s value matches that from the spectral method for $t \geq 30$. (b) Case $N = 32$. The OpenFOAM result with the standard C_s is an order of magnitude larger than that of the spectral method. A larger C_s is needed for the OpenFOAM result to match the reference solution.

evolution of the $k = 1$ iso-surface during the initial phase. Starting from an initial single wavenumber flow field, increasingly higher wavenumber structures appear as time progresses. In contrast, Fig. 7(b1)-(b3) focuses on the decay regime and show the evolution of the iso-surface for $k = 0.005$. As can be seen, the initial field has a similar single-wavelength structure, as in Fig. 7(a1), but at $t = 20$ the presence of small-scale turbulence is evident. At $t = 40$, these small-scale features diminish and flow structures dominated by lower frequencies become more prominent. A remarkable feature common to Fig. 7(a2), (a3), (b2) and (b3) is that the isosurfaces exhibit mirror symmetry with respect to the planes $x = 0$ and $y = 0$. Previous studies have reported that the evolving turbulent structures in the TGV flow maintain a symmetry nature over time (Brachet, 1991; Sharma and Sengupta, 2019; Sharma et al., 2020). The present OpenFOAM results are consistent with these findings. Although, as described in the previous chapter, the OpenFOAM analysis exhibits a small non-negligible inviscid conservation error, this error appears to have a negligible effect on the preservation of the symmetric structure of the flow

Figure 8 shows the time evolution of the spatially averaged turbulent kinetic energy, comparing the present OpenFOAM-based analysis with the spectral method. Here, K is the spatially averaged value of the kinetic energy $u_i u_i/2$ at each time step. The OpenFOAM results are further distinguished by different values of the Smagorinsky model constant, C_s. A Gaussian spatial filter corresponding to grid resolutions of $N = 128$ and $N = 32$ was applied a posteriori to the DNS velocity field. As shown in Fig. 8(a), for $N = 128$, the distribution for $C_s = 0.1$ in the OpenFOAM analysis agrees well with that of the spectral method when sufficient time has elapsed. Although the results for $C_s = 0$, 0.2, and 0.3 are also shown, these distributions deviate from the prediction of the spectral method, unlike the case of $C_s = 0.1$. For the $N = 128$ filter, the reduction in turbulent kinetic energy is negligible, as shown in the figure. Hence the previously established agreement between the high-resolution OpenFOAM LES and the DNS is unaffected by the filtering operation. These results suggest that despite the presence of a non-negligible inviscid conservation error in the OpenFOAM analysis, a sufficiently refined mesh ($N = 128$) allows for a reasonably accurate decay profile of turbulent kinetic energy under the commonly used Smagorinsky constant $C_s = 0.1$. Because the present test case is the TGV, the observed decay of the total turbulent kinetic energy is governed by a cascade that transports energy from the largest eddies to progressively smaller ones. This cascade is not merely a qualitative picture; it is tied directly to the shape of the energy spectrum in wavenumber space. A familiar example is the − 5/3 power law in the inertial sub-range. The SGS model constant is likewise linked to the spectral form. In the Smagorinsky model, for instance, the constant is proportional to the three-quarter power of Kolmogorov's constant—the prefactor of the − 5/3 spectrum—yielding the theoretical estimate $C_s \approx 0.17$. Because all runs share the same initial velocity field, increasing C_s steepens the spectral slope, forcing the energy density to fall more

[DOI: 10.1299/mej.25-00095]

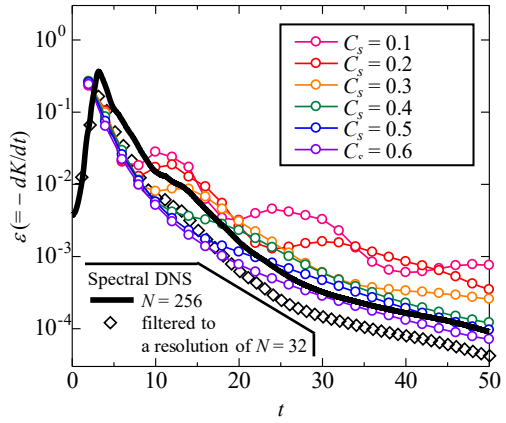

Fig. 9 Time evolution of the dissipation rate ε in the 3D viscous TGV flow obtained by the present OpenFOAM analysis, where $\varepsilon = -dK/dt$. The results for $N = 32$ are shown as a function of C_s and compared to the spectral method. As can be seen, a larger C_s than the default value is required for the OpenFOAM analysis to produce a dissipation profile equivalent to the spectral method.

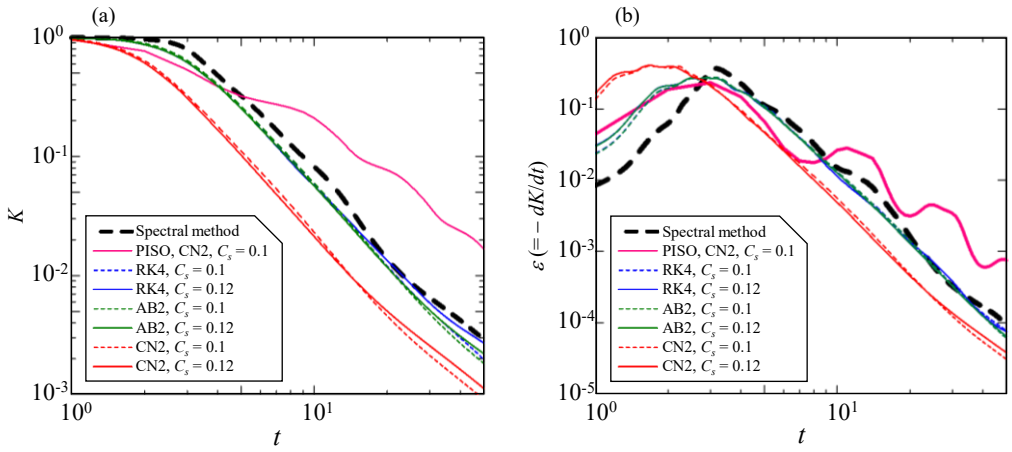

Fig. 10 Time evolution of turbulent kinetic energy and dissipation rate in the 3D viscous TGV flow obtained by the present OpenFOAM analysis. These results are compared with those obtained by a fractional-step method. Although the fractional-step method with an explicit time-integration scheme strictly preserves energy under inviscid conditions, the implicit scheme exhibits errors in inviscid energy conservation.

rapidly with wavenumber than in the reference spectral solution. When C_s is raised beyond the value consistent with the target spectrum, this artificially enhanced high-wavenumber damping can induce over-dissipation blocking: the energy transfer stalls near the grid cut-off, a spectral bottleneck forms, and the total turbulent kinetic energy rises transiently before resuming its decay.

Figure 8(b) compares the OpenFOAM-based turbulence kinetic energy distribution for $N = 32$ with that obtained by the spectral method. In contrast to the case shown in Fig. 8(a), the results for $C_s = 0.1$ are almost an order of magnitude larger than those obtained by the spectral method. Moreover, in this $N = 32$ case, matching the spectral method values requires increasing the Smagorinsky constant C_s to about 0.4-0.5, which is several times larger than the default value typically used in high-fidelity analyses. With the coarser $N = 32$ filter, kinetic energy decreases perceptibly, but only up to $t \approx 15$—that is, before the turbulence has decayed appreciably. Beyond $t = 25$, where the decay exponent is evaluated, the filtered $N = 32$ data remain close to the $N = 256$ DNS reference. From the spatially averaged turbulent kinetic energy K, the dissipation rate ε can be calculated as follows (Brachet et al., 1983; Brachet, 1991; Suzuki and Kouchi, 2022):

$$\varepsilon(t) = -dK(t)/dt. \tag{3}$$

[DOI: 10.1299/mej.25-00095]

Here, in this study this study has examined carefully how to evaluate the viscous dissipation rate, ε. Ultimately we use only its spatially averaged value to determine the turbulence-decay exponent. Because the spectral solver delivers a DNS solution whereas the OpenFOAM runs are LES, we sought a definition of ε that would not bias the comparison. Although numerical dissipation could in principle be quantified by subtracting the molecular and SGS contributions from ε, that residual would depend strongly on solver settings and on the instantaneous flow field, making it a fragile basis for firm conclusions. Following precedent in Taylor–Green vortex studies, we therefore compute ε from the global energy balance, $\varepsilon = -dK/dt$, and then obtain the decay exponent from this total dissipation rate. In this formulation ε comprises the molecular dissipation derived from the strain-rate tensor, the SGS dissipation, and any remaining numerical error. Figure 9 compares the dissipation rate distribution from the OpenFOAM analysis at $N = 32$ with that of the spectral method. The time history of the total viscous dissipation rate, $-dK(t)/dt$, is likewise compared in the figure. Here the influence of the $N = 32$ filter is more pronounced, which is expected because the dissipation involves the strain-rate tensor and is therefore weighted toward higher wavenumbers. As shown, the dissipation rates predicted by OpenFOAM for $C_s = 0.1$ and 0.2 exceed those of the spectral method by about an order of magnitude. Consistent with the kinetic energy comparisons, achieving a dissipation rate similar to the spectral method requires choosing C_s in the range of 0.4-0.5.

Figure 10 compares the time distributions of turbulent kinetic energy and dissipation rate for different analyses, focusing on the cases $C_s = 0.1$ and $C_s = 0.12$. The fractional-step LES results are shown alongside the present OpenFOAM-based analysis. As indicated, when the fractional-step LES employs the RK4 and AB2 time integration schemes, both of which preserve energy under inviscid conditions, the turbulent kinetic energy and dissipation rate profiles for $C_s = 0.1$ and $C_s = 0.12$ generally match those of the spectral method in the long-time decay regime. In contrast, when the CN2 is used, which introduces errors in the conservation property, the resulting distributions deviate from those of the spectral method. Additionally, the OpenFOAM-based results for $C_s = 0.1$ are shown for comparison. These results suggest that for $N = 32$, the accuracy of the energy conservation in the LES analysis significantly affects the calculated turbulent kinetic energy distribution.

The pattern by which kinetic-energy conservation errors manifest differs markedly between the inviscid and viscous test cases examined here. For the three-dimensional inviscid flow, the energy cascade should, by definition, transfer kinetic energy from large to small scales without viscous influence. When the discrete scheme fails to conserve kinetic energy, however, this transfer behaves as though an artificial diffusive (viscous-like) term were present. Such numerical diffusion therefore contaminates the cascade itself. A direct consequence is that the $-5/3$ power law of the inertial subrange—derived under the assumption of inviscid transport—may be distorted by the conservation error. In the viscous TGV problem, molecular viscosity is already active and is supplemented by the LES eddy viscosity. Any additional, non-physical diffusion produced by a conservation error thus acts on top of two genuine diffusion mechanisms. Excessive dissipation can trigger over-dissipation blocking (e.g., Sun and Yang, 2023), in which the cascade stalls and the inertial-range spectrum deviates strongly from the expected form. Although this phenomenon usually suppresses the overall turbulent kinetic energy, a coarse-grid LES of statistically unsteady turbulence (such as the present TGV flow) may instead experience a spectral energy pile-up near the grid cut-off. In that event the total kinetic energy can increase transiently, because energy is not transferred efficiently to the sub-grid scales. The increase is temporary—once integrated over a sufficiently long interval, the net energy dissipation is still reduced by the conservation error—but even a transient surplus may appreciably skew the resolved, grid-scale turbulence. Consequently, conservation errors remain a potential source of bias in unsteady LES, regardless of whether their effect on the total energy appears transient or persistent.

As shown in Fig. 9, the spatially averaged turbulent kinetic energy in the TGV flow, considered as a form of decaying turbulence, is expected to follow the following power-law decay behavior in the long-term decay regime (Pope, 2000; Mohamed and LaRue, 1990; Krogstad and Davidson, 2010; Kurian and Fransson, 2009; Suzuki et al., 2016):

$$K(t) = A\,(t - t_0)^{-n}. \tag{4}$$

where t_0 is a virtual origin, A is a decay coefficient and n is the decay exponent. The decay exponent is considered an important parameter that quantifies the decay characteristics of the turbulence and plays a role in forming one of the model constants in RANS analyses (Pope, 2000). Focusing on this exponent n, the present study verifies the performance of the OpenFOAM-based analysis. By using the viscous dissipation ε given by Eq. (3), the following turbulence time scale T is used in the present study (Suzuki at al., 2013b):

[DOI: 10.1299/mej.25-00095]

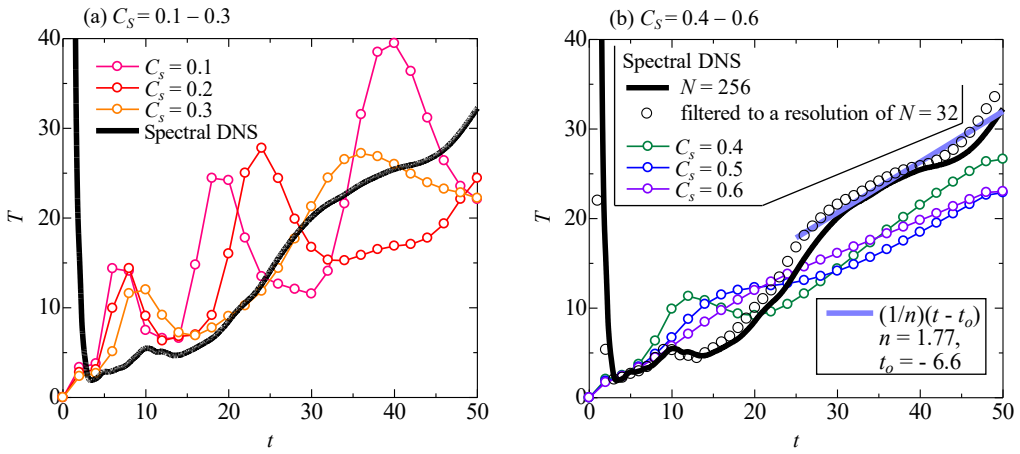

Fig. 11 Time evolution of the turbulent time scale as a function of C_s. (a) Results for C_s = 0.1 to 0.3. Unlike the spectral method, the OpenFOAM result for $t \geq 30$ does not vary linearly with time, but shows large variations. (b) Results for C_s = 0.4 to 0.6. For $t \geq 30$ the OpenFOAM result becomes an almost linear function of time. The value of the decay exponent from the spectral method is also shown.

$$T = K(t)/\varepsilon(t) = (1/n)\,(t - t_0). \tag{5}$$

which allows the determination of the decay exponent n if the turbulent kinetic energy does indeed follow the aforementioned power law. Figure 11(a) and 11(b) compares the temporal evolution of the turbulence time scale T from the OpenFOAM analysis with that from the spectral method. Figure 11(a) shows the results for C_s = 0.1-0.3, while Fig. 11(b) focuses on C_s = 0.4-0.6. As shown in Fig. 11(a), for C_s = 0.1-0.3, the turbulent time scale from the OpenFOAM analysis varies with time, so it does not seem appropriate to approximate it by the linear function given above. In contrast, the time scale distribution from the spectral method is approximately linear for $t \geq 30$. In a three-dimensional Taylor–Green vortex, as in other cases of decaying grid turbulence, small-scale fluctuations are expected to be sufficiently excited for $t \geq 30$, placing the flow in the viscous decay range while largely preserving the spectral shape. Although it would be ideal for the turbulent kinetic energy to follow a clear power-law, Fig. 11(b) shows that the turbulent time scale does not form a perfect straight line over t = 30-50. The interval t = 32–37, where the time-scale curve appears almost perfectly linear, was therefore selected; within this window a least-squares fit was applied to obtain the virtual origin and decay exponent. Some arbitrariness may remain in the choice of the fitting interval, yet Fig. 11(b) indicates that a straight-line approximation with the same slope (i.e., the same decay exponent) is also valid across $30 \leq t \leq 50$. Consequently, whether the fitting interval is set to t = 32–37 or to t = 30–50 changes only the virtual origin, exerting negligible influence on the estimated decay exponent. Because the conclusions of this work are based on the decay-exponent value, this freedom in choosing the fitting interval does not affect those conclusions. In Fig. 11(b), the spectral method distribution is fit by the above equation, yielding n = 1.77. Also plotted are the OpenFOAM results for C_s = 0.4–0.6, which show a roughly linear variation of the turbulent time scale for $t \geq 30$. These observations suggest that for large values of C_s, the mean turbulent kinetic energy obtained from OpenFOAM-based LES can indeed be described by a power-law decay. Here, the impact of the spatial filter on the decay exponent is assessed in the figure. Although the turbulence time scale derived from the N = 32-filtered field deviates slightly from the N = 256 DNS value, it still follows the linear relationship based on the decay exponent and virtual origin with excellent fidelity. Quantitatively, the differences introduced by the filter are too small to affect the study's main conclusions. The decay exponent of turbulent kinetic energy must be evaluated by a procedure that is independent of the assumed virtual origin. This requirement has been verified in grid-generated turbulence produced by wind-tunnel meshes. Building on that evidence, the present study derives the decay exponent from Eq. (5), which links the turbulent kinetic energy K to the total viscous dissipation rate $-dK(t)/dt$. Because Eq. (5) yields the decay exponent and the virtual origin simultaneously, the exponent is obtained without bias from any a priori choice of virtual origin (e.g., Suzuki et al., 2013b). For conventional square-mesh grid turbulence—where the kinetic-energy field is essentially uniform in space—the exponent is typically $n \approx 1.3$ (e.g., Mohamed and LaRue, 1990; Suzuki

[DOI: 10.1299/mej.25-00095]

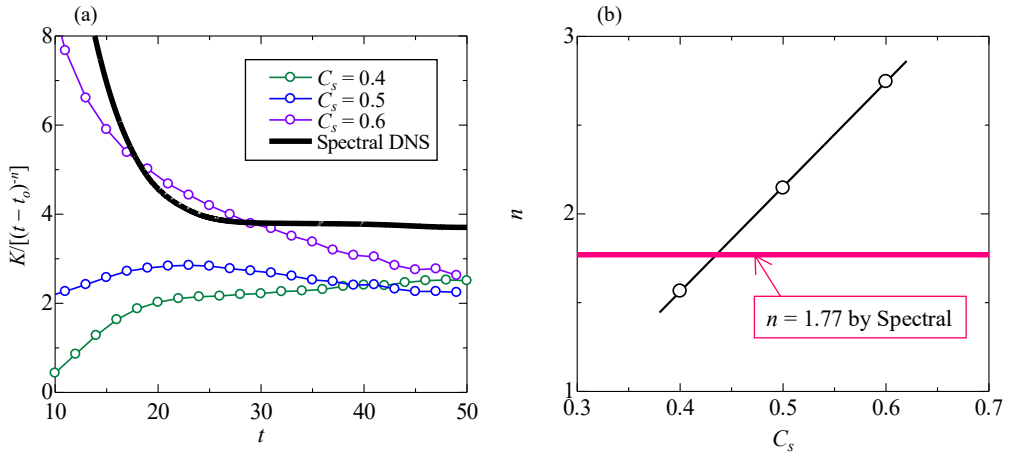

Fig. 12 (a) Time evolution of $K / [(t - t_o)^{-n}]$ from the OpenFOAM analysis compared to the spectral method, where $N = 32$. The spectral method shows a nearly constant profile for $t \geq 30$, while the OpenFOAM results increase or decrease with time depending on C_s. These results suggest that a value of C_s between 0.4 and 0.5 stabilizes the time profile. (b) Decay exponents obtained from the OpenFOAM analysis as a function of C_s, again compared to the spectral method. Here $N = 32$. As indicated, a value of C_s slightly larger than the default of 0.1 aligns the OpenFOAM decay exponent with that of the spectral approach.

et al., 2016, 2018). When the energy field is non-uniform, as in turbulence generated by multiscale grids, larger values around $n \approx 2$ (Nakamura et al., 2024) have been reported. The initial Taylor–Green vortex has a single spatial wavelength equal to the box length 2π and, as the visualisations demonstrate, exhibits marked spatial non-uniformity. It therefore yields a decay exponent higher than that observed for square-mesh grid turbulence, consistent with the behaviour reported here.

Figure 12(a) compares the decay law corresponding to a decay exponent $n = 1.77$ derived from the turbulent kinetic energy distribution of the spectral method with that obtained from the present OpenFOAM-based analysis. In the figure, if the distribution can be described by a power law whose exponent n matches that of the spectral method, then the quantity on the vertical axis remains constant with time. As shown in Fig. 12(a), this quantity decreases with time for $C_s = 0.5$ and 0.6 for $t \geq 30$, while it increases for $C_s = 0.4$. These observations imply that the value of C_s that makes the quantity on the vertical axis constant is between 0.4 and 0.5. Figure 12(b) plots the decay exponent n as a function of C_s for $C_s = 0.4$-0.6. As shown in the figure, matching the OpenFOAM-based decay exponent to that of the spectral method requires setting $C_s \approx 0.43$. Note that this value is several times larger than the Smagorinsky constant commonly used in high-fidelity analyses. Nevertheless, as demonstrated in the present study, when a reference solution is available, such as the results of the spectral method, adjusting C_s to match the turbulent kinetic energy distribution to the reference solution allows OpenFOAM to reproduce an equivalent turbulence decay characteristics.

The Smagorinsky coefficient, C_s, is not an arbitrary tuning knob but a numerical representation of inter-scale energy transfer. Consequently, its value must be chosen so that the LES reproduces the true cascade as faithfully as possible. The model constant of the Smagorinsky model has a theoretical formula (Lilly, 1967; Lesieur and Metais, 1996; Pope, 2000) as follows: $C_s \approx (1/\pi)\,(3\,C_K/2)^{-3/4}$. For example, when $C_K = 1.4$, C_s becomes 0.18. The value $C_s = 0.17$ is frequently used (Deardorff, 1971; Pope, 2000). In actual free-shear turbulence, C_s may be set to about 0.2 (Clark et al., 1979; Sagaut, 2006). Using experimental data (Comte-Bellot and Corrsin, 1971), C_s has been obtained as 0.19 – 0.24, as described in Rogallo and Moin (1984). On the other hand, it is recognized that a single universal C_s cannot represent all turbulent flows. In channel turbulence, $C_s = 0.1$ is commonly used (Deardorff, 1971; Pope, 2000; Sagaut, 2006). The value obtained by Lilly gives excessively large mean shear in channel turbulence (Deardorff, 1971). Therefore, when LES is applied to channel flow, $C_s = 0.1$ is adopted and is used as the standard empirical value for wall turbulence (Deardorff, 1970). The reason why the small value $C_s = 0.1$ is required in channel turbulence is that the mean velocity gradient is not zero and thus contributes to the magnitude of the strain rate (Sagaut, 2006). In fact, by subtracting the mean strain-rate tensor, it is possible to reproduce the turbulent field well even when a value close to the theoretical one is used in channel turbulence (Lévêque et al., 2007). The optimal value of C_s in channel turbulence may depend on spatial resolution. Only

[DOI: 10.1299/mej.25-00095]

when sufficiently fine grids are used can the value of C_s suitable for homogeneous turbulence (about 0.2) provide sustained resolved-scale motions (Mason and Callen, 1986). The consensus range $0.10 \leq C_s \leq 0.20$ therefore embraces the empirically optimal choices for most well-studied cases. Alternative derivations yield $C_s \approx 0.11$ (Yoshizawa, 1982). High-fidelity solvers—e.g. spectral codes or energy-conserving staggered-mesh schemes—introduce minimal numerical diffusion, so the SGS closure must supply the correct dissipation; selecting C_s within the accepted band is especially critical. In the present work, however, the optimum value that reconciles a coarse-mesh OpenFOAM LES with the spectral reference is $C_s = 0.43$, far outside the established interval. Reducing the first significant digit of 0.43 by one order of magnitude places it at $C_s \approx 0.14$, mid-way between 0.10 and 0.17; in other words, the chosen coefficient is roughly half an order of magnitude larger than normal practice. Such an anomalously large coefficient implies that the simulated cascade deviates substantially from the Kolmogorov picture. Specifically, the coarse-grid LES in OpenFOAM suffers from kinetic-energy conservation errors that trigger over-dissipation blocking: energy transport stalls near the grid cut-off, creating a spectral bottleneck. The unphysically large C_s compensates for this bottleneck by adding excessive SGS eddy viscosity, thereby restoring agreement with the spectral solution only through a non-physical mechanism. Although the present study focuses on LES, an analogy can be drawn with RANS practice, where model coefficients are often retuned to mask deficiencies in the turbulence model. Our findings suggest that energy-non-conserving LES solvers such as OpenFOAM impose a similar necessity: reliable predictions can require C_s values well beyond the conventional 0.1–0.2 band. Insisting on the standard range would leave the conservation error unmitigated and degrade the credibility of the LES results.

This study demonstrates that in low-resolution OpenFOAM LES simulations with energy conservation errors, it may be necessary to use a Smagorinsky constant C_s significantly larger than the commonly used range of 0.1-0.2 to ensure quantitative reliability of the turbulent kinetic energy. The conventional C_s values are derived from previous LES studies using highly accurate conservation schemes. When these conditions are not met, tuning C_s to match numerical or experimental reference data can improve the apparent quantitative reliability of the turbulence statistics. Furthermore, such adjustments of model constants are common in RANS simulations, where matching to reference values is used to improve the fidelity of numerical results. In particular, as observed in both the present and previous studies, increasing the grid resolution sufficiently can maintain reliable predictions of turbulent kinetic energy and lower-order statistics even in the presence of conservation errors. For the standard k–ε model, even subtle adjustments of the model constants can lead to large changes in key predictions such as velocity profiles or drag coefficients. Recent uncertainty-quantification work shows that variability in these constants can induce drag-coefficient fluctuations of up to ≈ 53 %, with the dissipation constant $C_{\varepsilon 2}$ alone accounting for roughly 69 % of the total variance (Liu et al., 2024). Free-jet studies highlight the same sensitivity. Because the standard k–ε formulation tends to under-predict the spread of round jets (Pope, 1978), many researchers have retuned its coefficients. Thies and Tam (1996), for example, recalibrated the constants against an extensive database of axisymmetric and non-axisymmetric jet experiments, and the issue remains topical today (Weaver and Mišković, 2021). Similar re-optimisation is routinely applied to more recent RANS closures. In the k–ω SST model, Sakamoto et al. (2024) assimilated full-scale measurements to tune the constants for ship-hydrodynamics applications, while Younoussi and Ettaouil (2024) fitted two SST coefficients to match stall-condition data for wind-turbine blades. These examples underscore that careful calibration of turbulence-model parameters is often essential for accurate engineering predictions. Such improvements in prediction accuracy can help to develop a clearer physical understanding of the flow of interest. The present work thus underscores the critical importance of properly tuning the model constant.

4. Conclusion

The objective of this study is to validate an OpenFOAM-based LES analysis from the perspective of energy conservation under inviscid conditions and the decay behavior of viscous turbulence. The analysis uses the PISO algorithm and employs a second-order Crank-Nicolson method for time integration along with a second-order central difference scheme for spatial discretization. The Smagorinsky model is adopted as the SGS model. For the inviscid case, two types of periodic box domains are investigated: two-dimensional and three-dimensional. In the two-dimensional flow, the velocity field is given by Taylor's analytical solution, while in the three-dimensional flow, the Taylor-Green vortex (TGV) is used. To verify the viscous decay behavior, the study focuses on a three-dimensional TGV flow with Re = 1600. The OpenFOAM results are compared with those obtained by a Fourier spectral method and a fractional-step

[DOI: 10.1299/mej.25-00095]

LES analysis. In the fractional-step LES, energy is conserved under inviscid conditions when using the explicit RK4 or AB2 time integration schemes, while the implicit CN method introduces a non-negligible energy conservation error. In examining this TGV flow, the grid resolution in the OpenFOAM-based analysis is set to N = 128 or 32, and the Smagorinsky model constant C_s is varied from 0 to 0.6.

It was confirmed that the flow can be made inviscid by asymptotically reducing the Smagorinsky model constant to zero. Although the two-dimensional results exhibit kinetic energy conservation errors, these errors decrease as the number of grid points increases. Subsequently, the same approach was applied to a three-dimensional inviscid TGV flow, showing that while OpenFOAM can handle an inviscid flow similarly, the kinetic energy conservation error does not decrease with increasing grid resolution. Next, the study evaluated the OpenFOAM-based analysis for a viscous TGV turbulent flow. The visualization results showed that despite the presence of conservation errors, the instantaneous flow field retains its symmetric structure. When the grid resolution is sufficiently high of N = 128, the OpenFOAM LES results obtained with the commonly used Smagorinsky constant of C_s = 0.1 agree well with those of the spectral method for $t \geq 30$. However, for a lower grid resolution of N = 32, the kinetic energy and dissipation rates predicted by the same model constant are about an order of magnitude higher than those from the spectral method. Comparisons with an LES analysis based on a fractional-step method and an evaluation from the point of view of turbulence decay confirm that setting $C_s \approx 0.43$, a value larger than the usual default, yields a decay exponent that matches that of the spectral method. In this study, the OpenFOAM results are benchmarked against reference solutions obtained with a spectral solver and a fourth-order central-difference scheme. Looking ahead, it would be worthwhile to investigate how the disparate formal accuracy of these spatial discretizations—and the attendant differences in effective resolution—might affect the conclusions drawn herein. Also, higher-order moments of the strain-rate tensor are, by themselves, critical for characterising the Smagorinsky closure. The present paper, however, concentrates on demonstrating that a larger model coefficient is required to compensate for kinetic-energy conservation errors. To keep that central conclusion clear, we have not included results for the higher-order strain-rate moments. Investigating those statistics remains a promising avenue for future work building on this study.

Acknowledgments

The authors are deeply grateful to Mr. Makoto Chitose (Okayama University) for his support in carrying out this work. This work was partly supported by the Japanese Ministry of Education, Culture, Sports, Science and Technology through Grants-in-Aid (Nos. 21K03859 and 22H01684). This work was supported by a research grant from the Kurita Water and Environment Foundation (Grant No. 25B042). This work was supported by a research grant from the Okayama Foundation for Science and Technology (Year 2025).

References

Asada, H., Maruyama, K. and Kawai, S., Temporal discretization for improving kinetic-energy and entropy preservation properties in KEEP schemes, Computers & Fluids, Vol. 270 (2024), p. 106143, DOI: 10.1016/j.compfluid.2023.106143.

Brachet, M. E., Meiron, D. I., Orszag, S. A., Nickel, B. G., Morf, R. H. and Frisch, U., Small-scale structure of the Taylor–Green vortex, Journal of Fluid Mechanics, Vol. 130 (1983), pp. 411-452.

Brachet, M., Direct simulation of three-dimensional turbulence in the Taylor–Green vortex, Fluid Dynamics Research, Vol. 8, No. 1-4 (1991), pp. 1-8.

Brener, B. P., Cruz, M. A., Thompson, R. L. and Anjos, R. P., Conditioning and accurate solutions of Reynolds average Navier–Stokes equations with data-driven turbulence closures, Journal of Fluid Mechanics, Vol. 915 (2021), A110, DOI: 10.1017/jfm.2021.148.

Canuto, C., Hussaini, M. Y., Quarteroni, A. and Zang, T. A., Spectral methods in fluid dynamics (1988), pp. 201-239, Springer.

Canuto, V. M. and Cheng, Y., Determination of the Smagorinsky–Lilly constant C_S, Physics of Fluids, Vol. 9, No. 5 (1997), pp. 1368-1378.

Cao, Y. and Tamura, T., Large-eddy simulations of flow past a square cylinder using structured and unstructured grids, Computers & Fluids, Vol. 137 (2016), pp. 36-54.

[DOI: 10.1299/mej.25-00095]

Chitose, M., Suzuki, H. and Kouchi, T., Attempt to compensate for effects of energy conservation error on static pressure fluctuation using sub-grid scale components with the Reynolds number dependence of isotropic/anisotropic steady turbulence, Journal of Physics: Conference Series, Vol. 2793, No. 1 (2024), p. 012004, DOI: 10.1088/1742-6596/2793/1/012004.

Choi, H. and Moin, P., Effects of the computational time step on numerical solutions of turbulent flow, Journal of Computational Physics, Vol. 113, No. 1 (1994), pp. 1-4.

Clark, R. A., Ferziger, J. H. and Reynolds, W. C., Evaluation of subgrid-scale models using an accurately simulated turbulent flow, Journal of Fluid Mechanics, Vol. 91, No. 1 (1979), pp. 1-16.

Comte-Bellot, G. and Corrsin, S., Simple Eulerian time correlation of full- and narrow-band velocity signals in grid-generated isotropic turbulence, Journal of Fluid Mechanics, Vol. 48, No. 2 (1971), pp. 273-337.

Deardorff, J. W., A numerical study of three-dimensional turbulent channel flow at large Reynolds numbers, Journal of Fluid Mechanics, Vol. 41, Part 2 (1970), pp. 453-480.

Deardorff, J. W., On the magnitude of the subgrid-scale eddy coefficient, Journal of Computational Physics, Vol. 7, No. 1 (1971), pp. 120-133.

Drikakis, D., Fureby, C., Grinstein, F. F. and Youngs, D., Simulation of transition and turbulence decay in the Taylor–Green vortex, Journal of Turbulence, Vol. 8 (2007), p. N20, DOI: 10.1080/14685240701250289.

Feng, Z., Qi, H., Huang, X., Liu, S. and Liu, J., Comparisons of subgrid-scale models for OpenFOAM large-eddy simulation, Journal of Physics: Conference Series, Vol. 1802, No. 4 (2021), p. 042088, DOI: 10.1088/1742-6596/1802/4/042088.

Harlow, F. H. and Welch, J. E., Numerical calculation of time-dependent viscous incompressible flow of fluid with free surface, Physics of fluids, Vol. 8, No. 12 (1965), pp. 2182-2189.

Honda, R., Suzuki, H. and Mochizuki, S., Time-series observation of the effects of kinetic energy conservation error on isotropic and anisotropic steady incompressible turbulence, Journal of Physics: Conference Series, Vol. 1978, No. 1 (2021), p. 012026, DOI: 10.1088/1742-6596/1978/1/012026.

Jasak, H., OpenFOAM: Open source CFD in research and industry. International Journal of Naval Architecture and Ocean Engineering, Vol. 1, No. 1 (2009), pp. 89-94.

Jiang, H. and Cheng, L., Large-eddy simulation of flow past a circular cylinder for Reynolds numbers 400 to 3900, Physics of Fluids, Vol. 33, No. 3 (2021), p. 034119, DOI: 10.1063/5.0041168.

Kajzer, A., Pozorski, J. and Szewc, K., Large-eddy simulations of 3D Taylor-Green vortex: Comparison of smoothed particle hydrodynamics, lattice Boltzmann and finite volume methods, Journal of Physics: Conference Series, Vol. 530, No. 1 (2014), p. 012019, DOI: 10.1088/1742-6596/530/1/012019.

Kim, J. and Moin, P., Application of a fractional-step method to incompressible Navier-Stokes equations, Journal of Computational Physics, Vol. 59, No. 2 (1985), pp. 308-323.

Kobayashi, H., The subgrid-scale models based on coherent structures for rotating homogeneous turbulence and turbulent channel flow, Physics of Fluids, Vol. 17, No. 4 (2005), p. 045104, DOI: 10.1063/1.1874212.

Komen, E., Shams, A., Camilo, L. and Koren, B., Quasi-DNS capabilities of OpenFOAM for different mesh types, Computers & Fluids, Vol. 96 (2014), pp. 87-104.

Krogstad, P. Å. and Davidson, P. A., Is grid turbulence Saffman turbulence?, Journal of Fluid Mechanics, Vol. 642 (2010), pp. 373-394.

Kurian, T. and Fransson, J. H. M., Grid-generated turbulence revisited, Fluid Dynamics Research, Vol. 41, No. 2 (2009), p. 021403, DOI: 10.1088/0169-5983/41/2/021403.

LarKermani, E., Roohi, E. and Porté-Agel, F., Evaluating the modulated gradient model in large eddy simulation of channel flow with OpenFOAM, Journal of Turbulence, Vol. 19, No. 7 (2018), pp. 600-620.

Lehmkuhl, O., Houzeaux, G., Owen, H., Chrysokentis, G. and Rodríguez, I., A low-dissipation finite element scheme for scale resolving simulations of turbulent flows, Journal of Computational Physics, Vol. 390 (2019), pp. 51-65.

Lesieur, M. and Métais, O., New trends in large-eddy simulations of turbulence, Annual Review of Fluid Mechanics, Vol. 28 (1996), pp. 45-82.

Lévêque, E., Toschi, F., Shao, L. and Bertoglio, J.-P., Shear-improved Smagorinsky model for large-eddy simulation of wall-bounded turbulent flows, Journal of Fluid Mechanics, Vol. 570 (2007), pp. 491-502.

Lilly, D. K., The representation of small-scale turbulence in numerical simulation experiments, Proceedings of the IBM Scientific Computing Symposium on Environmental Sciences, IBM Data Processing Division, White Plains, N.Y.,

[DOI: 10.1299/mej.25-00095]

(1967), pp. 195-210.

Liu, H., Kong, Z., Li, G., Chen, C., Zhao, Y. and Zhang, S., Uncertainty quantification of the standard k–ε turbulence-model closure coefficients in predicting aerodynamics of a high-speed train, Engineering Applications of Computational Fluid Mechanics, Vol. 18, No. 1 (2024), p. 2430658, DOI: 10.1080/19942060.2024.2430658.

Mason, P. J. and Callen, N. S., On the magnitude of the subgrid-scale eddy coefficient in large-eddy simulations of turbulent channel flow, Journal of Fluid Mechanics, Vol. 162 (1986), pp. 439-462.

Meneveau, C. and Katz, J., Scale-invariance and turbulence models for large-eddy simulation, Annual Review of Fluid Mechanics, Vol. 32, No. 1 (2000), pp. 1-32.

Menter, F. R., Review of the shear-stress transport turbulence model experience from an industrial perspective, International Journal of Computational Fluid Dynamics, Vol. 23, No. 4 (2009), pp. 305-316.

Mohamed, M. S. and LaRue, J. C., The decay power law in grid-generated turbulence. Journal of Fluid Mechanics, Vol. 219 (1990), pp. 195-214.

Morinishi, Y., Lund, T. S., Vasilyev, O. V. and Moin, P., Fully conservative higher order finite difference schemes for incompressible flow, Journal of Computational Physics, Vol. 143, No. 1 (1998), pp. 90-124.

Morinishi, Y. and Vasilyev, O. V., Vector level identity for dynamic subgrid scale modeling in large eddy simulation, Physics of Fluids, Vol. 14, No. 10 (2002), pp. 3616-3623.

Morinishi, Y., Yamaki, M., Obata, T. and Takeichi, K., Numerical method for LES of incompressible flow with compact finite difference, Transactions of the Japan Society of Mechanical Engineers Series B, Vol. 77, No. 781 (in Japanese) (2011), pp. 1731-1746.

Muhammad, N., Lashin, M. M. and Alkhatib, S., Simulation of turbulence flow in OpenFOAM using the large eddy simulation model, Proceedings of the Institution of Mechanical Engineers, Part E: Journal of Process Mechanical Engineering, Vol. 236, No. 5 (2022), pp. 2252-2265.

Nakamura, K., Suzuki, H., Kouchi, T. and Tanaka, K., RANS model-based constant-temperature anemometry examination to validate negligible wind-tunnel blockage effect on developed multi-scale grid turbulence, Proceedings of the 3rd International Conference on Automation, Robotics and Computer Engineering (ICARCE) (2024), pp. 453-457.

Ono, A., Suzuki, H., Kouchi, T. and Tanaka, K., Numerical analysis validating the standard k-epsilon model for the kinetic energy of turbulence subjected to weak but long-lasting wind tunnel blockage acceleration, Journal of Fluid Science and Technology, Vol. 20, No. 1 (2025), p. JFST0004, DOI: 10.1299/jfst.2025jfst0004.

Park, N., Lee, S., Lee, J. and Choi, H., A dynamic subgrid-scale eddy viscosity model with a global model coefficient, Physics of Fluids, Vol. 18, No. 12 (2006), p. 125109, DOI: 10.1063/1.2401626.

Pope, S. B., An explanation of the turbulent round-jet / plane-jet anomaly, AIAA Journal, Vol. 16, No. 3 (1978), pp. 279-281.

Pope, S. B., Turbulent flows (2000), Cambridge University Press.

Robertson, E., Choudhury, V., Bhushan, S. and Walters, D. K., Validation of OpenFOAM numerical methods and turbulence models for incompressible bluff body flows, Computers & Fluids, Vol. 123 (2015), pp. 122-145.

Rogallo, R. S. and Moin, P., Numerical simulation of turbulent flows, Annual Review of Fluid Mechanics, Vol. 16 (1984), pp. 99-137.

Sagaut, P., Large Eddy Simulation for Incompressible Flows, 3rd ed. (2006), Springer.

Sakamoto, N., Hino, T., Kobayashi, H. and Ohashi, K., Parameter adaptation of the k–ω SST turbulence model for improving resolution of moderately separated flows around a 2-D wing and 3-D ship hulls via EnKF data assimilation, Journal of Marine Science and Technology, Vol. 29, No. 4 (2024), pp. 885-909.

Sharma, N. and Sengupta, T. K., Vorticity dynamics of the three-dimensional Taylor-Green vortex problem, Physics of Fluids, Vol. 31, No. 3 (2019), p. 035106, DOI: 10.1063/1.5083870.

Sharma, N., Sengupta, T. K. and Brinkerhoff, J. R., Non-linear instability analysis of the three-dimensional Navier–Stokes equations: Taylor–Green vortex problem, Physics of Fluids, Vol. 32, No. 6 (2020), p. 064102, DOI: 10.1063/5.0006683.

Shirzadi, M., Mirzaei, P. A. and Tominaga, Y., RANS model calibration using stochastic optimization for accuracy improvement of urban airflow CFD modeling, Journal of Building Engineering, Vol. 32 (2020), p. 101756, DOI: 10.1016/j.jobe.2020.101756.

[DOI: 10.1299/mej.25-00095]

Shu, C. W., Don, W. S., Gottlieb, D., Schilling, O. and Jameson, L., Numerical convergence study of nearly incompressible, inviscid Taylor–Green vortex flow, Journal of Scientific Computing, Vol. 24 (2005), pp. 1-27.

Song, X., Yu, Z., Liu, C. and Cheng, G., Calibration of RANS model constant based on data assimilation and accurate simulation of separated flow, AIP Advances, Vol. 12, No. 9 (2022), p. 095324, DOI: 10.1063/5.0103253.

Spalart, P. R., Strategies for turbulence modelling and simulations, International Journal of Heat and Fluid Flow, Vol. 21, No. 3 (2000), pp. 252-263.

Sun, G. and Yang, L., Large eddy simulations of turbulent flow based on a removal of energy production through nonlinear interactions, Physics of Fluids, Vol. 35, No. 1 (2023), p. 015145, DOI: 10.1063/5.0133801.

Suzuki, H., Nagata, K., Sakai, Y., Hayase, T., Hasegawa, Y. and Ushijima, T., An attempt to improve accuracy of higher‐order statistics and spectra in direct numerical simulation of incompressible wall turbulence by using the compact schemes for viscous terms, International Journal for Numerical Methods in Fluids, Vol. 73, No. 6 (2013a), pp. 509-522.

Suzuki, H., Nagata, K., Sakai, Y., Hayase, T., Hasegawa, Y. and Ushijima, T., Direct numerical simulation of fractal-generated turbulence, Fluid Dynamics Research, Vol. 45, No. 6 (2013b), p. 061409, DOI: 10.1088/0169-5983/45/6/061409.

Suzuki, H., Mochizuki, S. and Hasegawa, Y., Validation scheme for small effect of wind tunnel blockage on decaying grid-generated turbulence, Journal of Fluid Science and Technology, Vol. 11, No. 3 (2016), p. JFST0012, DOI: 10.1299/jfst.2016jfst0012.

Suzuki, H., Hattori, S. and Mochizuki, S., Numerical investigation using an exact solution of the effects of non-solenoidality of the viscous terms on the incompressible flow, Journal of Fluid Science and Technology, Vol. 12, No. 1 (2017), p. JFST0001, DOI: 10.1299/jfst.2017jfst0001.

Suzuki, H., Mochizuki, S. and Hasegawa, Y., Numerical-based theoretical analysis on effects of weak fluid acceleration of free-stream due to wind-tunnel blockage on grid-generated turbulence, Flow Measurement and Instrumentation, Vol. 62 (2018), pp. 1-8.

Suzuki, H., Hasebe, K., Hasegawa, Y. and Ushijima, T., Reduced conservation error of kinetic energy using a Runge-Kutta algorithm with reduced numerical dissipation, Journal of Physics: Conference Series, Vol. 1633, No. 1 (2020a), p. 012021, DOI: 10.1088/1742-6596/1633/1/012021.

Suzuki, H., Hasegawa, Y., Watanabe, M., Ushijima, T. and Mochizuki, S., Second-order kinetic-energy-conservative analysis of incompressible turbulence under a collocated grid system, Journal of Physics: Conference Series, Vol. 1633, No. 1 (2020b), p. 012063., DOI: 10.1088/1742-6596/1633/1/012063.

Suzuki, H. and Kouchi, T., Development of a single-scale initial flow field into steady homogeneous turbulence with validating a constructed Fourier spectral analysis, Journal of Physics: Conference Series, Vol. 2313, No. 1 (2022), p. 012008, DOI: 10.1088/1742-6596/2313/1/012008.

Suzuki, H. and Hasegawa, Y., Dynamic subgrid-scale model constant-value estimation refined by vector-level identity in an atmospheric flow field, Journal of Fluid Science and Technology, Vol. 19, No. 4 (2024), p. JFST0035, DOI: 10.1299/jfst.2024jfst0035.

Thies, A. T. and Tam, C. K. W., Computation of turbulent axisymmetric and non-axisymmetric jet flows using the k–ε model, AIAA Journal, Vol. 34 (1996), pp. 309-316.

Weaver, D. S. and Mišković, S., A study of RANS turbulence models in fully turbulent jets: a perspective for CFD-DEM simulations, Fluids, Vol. 6, No. 8 (2021), p. 271, DOI: 10.3390/fluids6080271.

Xiao, H. and Cinnella, P., Quantification of model uncertainty in RANS simulations: A review, Progress in Aerospace Sciences, Vol. 108 (2019), pp. 1-31.

Younoussi, S. and Ettaouil, A., Calibration method of the k–ω SST turbulence model for wind-turbine performance prediction near stall condition, Heliyon, Vol. 10, No. 1 (2024), e24048, DOI: 10.1016/j.heliyon.2024.e24048.

Yoshizawa, A., A statistically-derived subgrid model for the large-eddy simulation of turbulence, The Physics of Fluids, Vol. 25, No. 9 (1982), pp. 1532-1538.

[DOI: 10.1299/mej.25-00095]